Gold Nanoparticle Deposition on Silica Nanohelices: A New Controllable 3D Substrate in Aqueous Suspension for Optical Sensing

ARTICLE *in* THE JOURNAL OF PHYSICAL CHEMISTRY C · NOVEMBER 2012

Impact Factor: 4.77 · DOI: 10.1021/jp307784m

THE JOURNAL OF PHYSICAL CHEMISTRY C

Article

pubs.acs.org/JPCC

Gold Nanoparticle Deposition on Silica Nanohelices: A New Controllable 3D Substrate in Aqueous Suspension for Optical Sensing

Rumi Tamoto,[†,‡] Sophie Lecomte,[†] Satyabrata Si,[§] Simona Moldovan,[∥] Ovidiu Ersen,[∥] Marie-Hélène Delville,[§] and Reiko Oda*[,†,‡]

[†]Chimie Biologie des Membranes et Nanoobjets, Université Bordeaux 1-CNRS UMR 5248, Allée, St Hilaire, Bat B14, 33607 Pessac, France

[‡]Institut Européen de Chimie et Biologie, 2 rue Robert Escarpit, 33607 Pessac, France

[§]CNRS, Université de Bordeaux, ICMCB, 87 avenue du Dr. A. Schweitzer, Pessac, F-33608, France

[∥]Institut de Chimie et de Physique des Matériaux de Strasbourg, CNRS, Université de Strasbourg, UMR 7504, 23 rue du Loess BP 43, 67034 STRASBOURG Cedex 2 France

Supporting Information

ABSTRACT: We describe new methods to prepare gold nanoparticle/silica nanohelix hybrid nanostructures which form a 3D network in the aqueous phase. Nanometric silica helices and tubules obtained by sol−gel polycondensation on organic templates of self-assembled amphiphilic molecules were further functionalized with (3-aminopropyl)-triethoxysilane (APTES) or (3-mercaptopropyl)triethoxysilane (MPTES). These helices interact strongly with gold nanoparticles (GNPs) of various diameters (1−15 nm). Small GNPs (1−2 nm) at the surface of silica nanohelices grew to about 5 nm when stored in the appropriate organic solvent, whereas this growth process was not observed in water, allowing the size of GNPs at the surface of silica to be controlled by a simple solvent exchange. Larger GNPs (more than 10 nm) at the surface of nano hybrid fibers were used to produce surface enhanced raman scattering (SERS) using benzenthiol as a probe. This provides a novel sustainable approach for designing nanohybrid systems with photonic applications such as ultrasensitive chemical and biological sensors using a simple aqueous suspension of a 3D network of nanohelices.

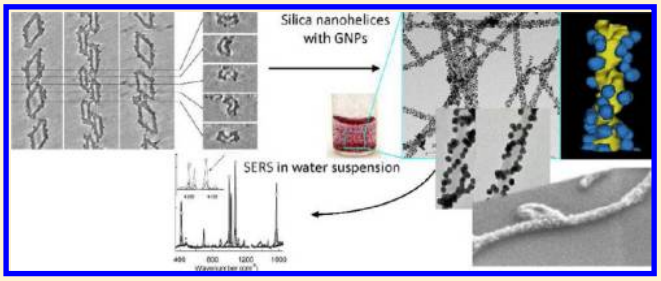

INTRODUCTION

The morphological and functional diversity of inorganic nanostructures found in nature has inspired the scientific community to explore their potential use in the development of materials,[1,2] for nanoscale electronics and sensing devices.[3−6] While nature is far ahead in terms of structural complexity of bioinorganic structures, the lack of fine-tunability of these objects calls for the development of synthetic methods enabling the controlled preparation of artificial nanosized architectures.[7−10] One of such methods is inspired from the structural diversity of self-assembled organic systems and exploits them as templates for the formation of inorganic nanomaterials.[11−16] Indeed, self-assemblies of small molecules or biomolecules[17−21] have given rise to a broad diversity of nanometric organic templates. This approach has been successfully used for the preparation of silica materials with various architectures[22−24] and/or controlled porosities,[25,26,10] via the sol−gel polycondensation of tetraethoxysilane (TEOS).

Among these various nanostructures, chiral self-assemblies such as twisted or helical ribbons and tubules have been the subject of increasing attention[27,28] and have been used as templates for the formation of chiral silica structures.[2] Indeed, these structures which provide well-defined nanoscale cavities with a confined environment suitable for the development of nanocontainers are under intensive investigation because of their potential utility as adsorbents and catalysts as well as their use in electronic devices.[29]

The great advantage of 3D morphologies (helices and twisted ribbons, tubules) compared to traditional 1D nanostructures (flat ribbons or wires) is based on their extremely high surface to volume ratio. Furthermore, nanohelices can exhibit unconventional physical properties due to their periodic helical structure and their flexibility, ideal for inducing polarization effects under mechanical stress.[30] Therefore, these nanoobjects can be considered as useful building blocks for constructing functional nanodevices.[31,32] The complexities and polymorphisms of these nanoobjects have also made ideal structures as templates for hybrid nanostruc-

Received: August 6, 2012
Revised: September 26, 2012
Published: October 9, 2012

   dx.doi.org/10.1021/jp307784m | J. Phys. Chem. C 2012, 116, 23143−23152

Table 1. TEM Images of GNP/Silica Helices Obtained under Various Conditions (the GNP Stabilizers and Functional Group of the Surface of Silica Nanohelices)[a]

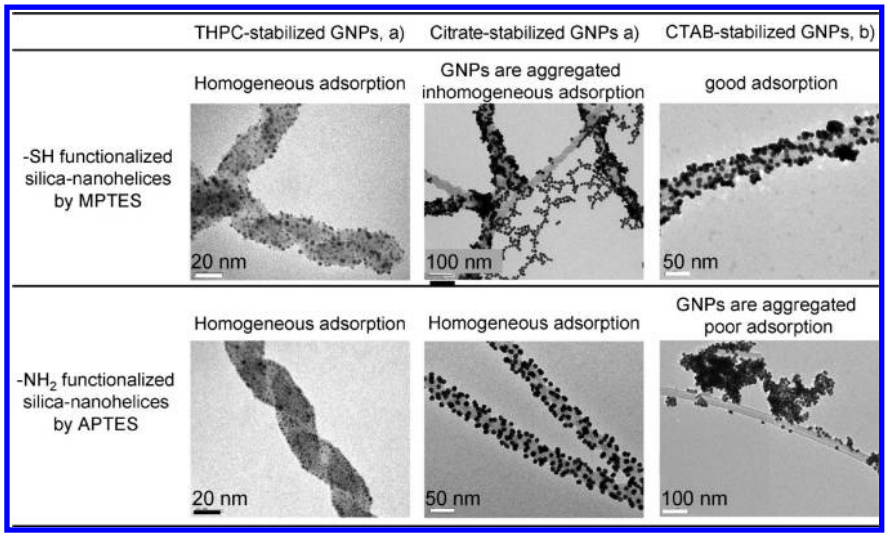

[a]a) Suspension in water; b) water/ethanol (1/1).

tures via various methods such as sol−gel transcription. In some cases, these hybrid chiral structures allowed transfer of chirality from organic to hybrid structures as studied by circular dichroism.[33,34] We have reported the synthesis of chiral nanometric silica ribbons, helices and tubes with tunable shapes based on self-assembled amphiphilic molecules.[35] These amphiphiles are cationic bis-quaternary ammonium gemini surfactants of chemical formula C_2H_4-1,2-$((CH_3)_2N^+C_{16}H_{33})_2$, noted hereafter 16−2−16, in the presence of tartrate counteranions, which form a gel in water by creating an extended network of nanometric twisted or helical ribbons or tubules with tunable chirality, shapes, and sizes.[36−38] Various parameters such as the temperature, the solvent, or the reactant concentrations have distinct effects on their structures. We also showed that the relative kinetics of the formation of these organic assemblies on one hand and the inorganic polycondensation on the other hand have remarkable effects on the final morphologies of the inorganic nanostructures.[35]

Recently, organization of noble metal nanoparticles on 1D or 2D surfaces has attracted great attention because of their resulting physical properties. When assembled close to each other, their localized surface plasmon resonances are coupled together, resulting in the enhancement of the electric field in the gap between the adjacent nanoparticles.[39−41] Such systems, therefore, are attractive candidates for the amplification of optical signals, including fluorescence,[42,43] Raman scattering,[44−47] and second-harmonic generation.[48] The amplification of Raman scattering (SERS spectroscopy) is especially useful for the detection of biological compounds at very low concentrations. SERS provides rich spectral and structural information about molecules when adsorbed on noble metal substrates, allowing a fine analysis of fluids, blood, tissues, and dye molecules, providing many potential applications for biomedical sensing, immunoassays,[49] optically triggered drug delivery,[50] and simultaneous cancer imaging.[51] SERS substrates are typically made of assembled metal nanoparticles on a planar surface or a patterned surface.[39,52−55] The optical property induced by the localized surface plasmon wavelength strongly depends on the local environment (particle size, shape, composition, and surface coating). More recently, substrates having other morphologies than two-dimensional surfaces have been developed, and among these various structures, hybrid ones based on silica nanofibers[56,57] or nanohelices[58] have attracted interest, as they can be used as bases for alignment of nanoparticles. However, all these nanostructures are still deposited on flat surfaces. Supramolecular self-assembly provides an alternative bottom-up approach giving rise to controllable nanostructures as bases for SERS substrates. In particular, for chiral nanostructures, the self-assembly route allows us to access controlled helical pitch and/or enantioselective structures. Recently, a number of systems were reported in which DNA or peptides are used to direct GNP in controlled organizations.[59−61] In some cases, the chirality of DNA is reflected in the organization of GNPs.[62−64]

In this study, we take advantage of the chiral nanohelices with tunable pitch and shape obtained by surfactant self-assemblies as described above, to prepare new hybrid nanostructures with GNPs of various sizes (1−14 nm). The details of these nanohybrid structures were characterized by tomography TEM. We show that very small GNPs (1.5 nm) deposited on such helical surfaces are very stable in water dispersion, whereas they can grow into larger size in alcoholic dispersion. We studied SERS of benzenethiol in the presence of GNPs (10−14 nm size) deposited on silica nanohelices and observed an important enhancement of the Raman signal. The unambiguous advantage of the present study is to illustrate the concept of the ability to perform SERS detection directly in liquid suspensions. The helical nanoobjects provide a 3D structure formation for ultrasensitive chemical and biological sensors.

■ RESULTS AND DISCUSSION

We have optimized new preparation methods of hybrid nanostructures based on gold nanoparticles (GNPs) and silica nanohelices. Two types of functionalization were used to chemically modify the silica nanohelix surfaces using either (3-aminopropyl)triethoxysilane (APTES) or (3-mercaptopropyl)-triethoxysilane (MPTES). Two approaches were adopted to synthesize GNPs with various sizes (1−15 nm) depending on the targeted size. The first one consisted of preparing gold

dx.doi.org/10.1021/jp307784m | J. Phys. Chem. C 2012, 116, 23143−23152

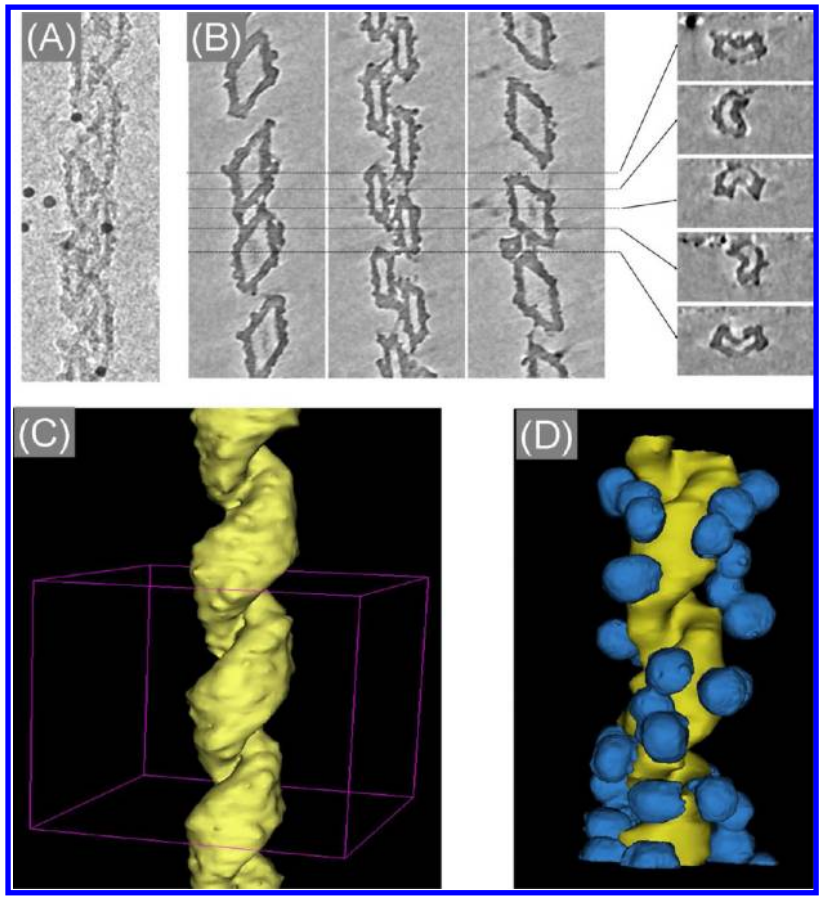

Figure 1. (A) Typical TEM image from the tilt series used to reconstruct the volume of a silica helix. (B) Examples of longitudinal (left) and transversal (right) slices extracted from the reconstruction, taken at equidistant distances. (C and D) 3D models obtained by the tomographic analysis of the silica helix and silica−gold nanohybrid (10 nm) structure, respectively.

nanoparticles of the desired size in the bulk solution using citrate or cetyltrimethylammonium bromide (CTAB) as stabilizers and performing their further deposition on the modified helices. The second one aimed at generating very small GNPs (1.1 nm) via a stabilization with tetrakis-(hydroxymethyl) phosphonium chloride (THPC), whose sizes could be increased after deposition on the silica helices.

GNPs Adsorbed on Silica Nanohelices. These gold NPs stabilized with different ligands were mixed with the chemically modified silica nanohelices (APTES and MPTES). In typical experiments, suspensions of 0.12 wt % of the chemically modified silica nanohelices transcribed from 1 mM organic gel were prepared in water (10−50 μL) and added into 200 μL of the GNP suspensions under ultrasonication. The respective concentrations of gold salts were 0.50 mM for citrate, 0.97 mM for THPC, and 0.25 mM for CTAB-stabilized GNPs. The results of the different reactions are summarized in Table 1.

The results from Table 1 show that the homogeneity of the adsorption of GNPs is particle size dependent. For 1−2 nm size THPC-stabilized nanoparticles, there is no difference in between the nature of the silica functional groups (−SH or NH_2). Both types of silica are homogeneously covered.[65] The pH of the silica suspension is around 6−8. Since alkylamines exist predominantly as positively charged R−NH_3^+ groups at pH < 10, the interaction between the ammonium groups and the negatively charged THPC gold nanoparticles[66] is mainly electrostatic rather than coordinative in nature. On the other hand, interactions between gold nanoparticles and thiol groups are more likely coordinative than electrostatic.

For **bigger size nanoparticles** (citrate and CTAB-stabilized GNPs), there is a competition between these stabilizing ligands and the amino or thiol groups on the silica surface. When different processes of bindings compete, the binding leading to the maximum decrease in the surface energy prevails. With respect to the energy of stabilization, the interaction strength follows the order of the chemical bond strength: S−Au interaction > N−Au interaction > carboxylate−Au interaction. Furthermore, citrate provides negative interfacial charge on each GNP,[67] whereas CTAB forms a positively charged bilayer around the GNP.

Therefore, the interaction of GNPs with the silica surface strongly depends on the ability of the amino/thiol modified surface of silica helices to displace the stabilizer at the surface of the GNPs.

The adsorption of citrate stabilized GNPs to the silica nanohelices depended strongly on the functional groups (−SH or NH_2). The GNPs showed a homogeneous distribution over the APTES silica helices due to electrostatic attractive interaction between ammonium (silica nanohelices) and citrate (GNPs), whereas, in the presence of thiol-functionalized silica nanohelices, these GNPs showed strong local aggregation.[65]

The CTAB-stabilized GNPs showed a poor adsorption in pure water both for APTES and MPTES functionalized silica. This is probably because of the high stability of the CTAB bilayers around the particles in water and its high concentration

dx.doi.org/10.1021/jp307784m | J. Phys. Chem. C 2012, 116, 23143−23152

in the bulk solution. If the silica is dispersed in a 1:1 mixture of water and ethanol, the CTAB double layer is partly destroyed due to the solubility of CTAB in ethanol, and a homogeneous and good adsorption of the GNPs is observed on the MPTES silica surface (Table 1, line 1). However, in the presence of APTES functionalized silica, these GNPs aggregated due to the combined effect of charge repulsion between amine groups (APTES from silica) and quaternary ammonium (CTAB from GNPs). How the reactants are mixed in the reaction medium is also crucial for the quality of GNP/silica helix hybrids. We have indeed observed that, in all cases, the coverage is much more homogeneous when the silica nanohelices are added into the GNP solution than the other way around (Figure S1 in the Supporting Information).

To study the morphology of silica helices and the distribution of gold nanoparticles on this support, electron tomography (ET) experiments have been carried out on several representative nano-objects. The results are summarized in Figure 1. The analysis of the transversal and longitudinal slices extracted from the 3D reconstruction (Figure 1B) allowed us to precisely quantify their morphological characteristics: we have obtained thus 45 nm for the helical periodicity, 5 ± 2 nm for the silica walls, and 4 ± 2 nm between the two walls. The silica surface roughness constitutes an appropriate condition for SERS signal enhancement. Concerning the spatial distribution of gold nanoparticles, the 3D analysis of the reconstructed volume of the gold–silica nanohybrid architecture (Figure 1D) has clearly shown that the nanoparticles grow principally on the external surface of the helices. They also seem to form clusters of roughly 3–4 particles generating potential hot spots for SERS applications, as will be discussed below.

At the surfaces of some of the helices, we also observed helical organization of GNPs (Figure 2). Although, for the

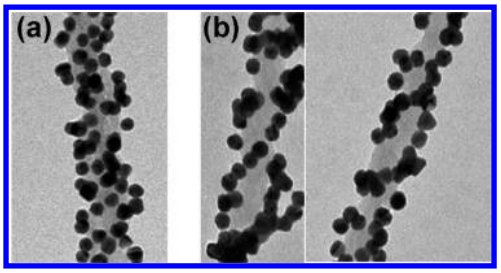

Figure 2. Helical organization of GNPs observed at the surfaces of nanohelices. Most of the helices show randomly adsorbed GNPs on the surface of silica helices (a), but some of the helices show helically organized GNPs (b).

moment, these structures are not the majority, if the adsorption of GNPs can be controlled in a chiral way, such structures will have very interesting potential applications.

The Growth of Small GNPs at the Surface of Silica Nanohelices. We also observed that the stabilization of the size of these GNPs adsorbed on the silica surface is strongly solvent dependent. Interestingly, when dispersed in alcohol suspension, the THPC-stabilized 1 nm GNPs adsorbed at the surface of the helices could increase their size up to 5 nm even in the absence (starvation process) of gold salt, whereas in water they are stable and remain ~1 nm for weeks. In Figure 2, we show the growth of GNPs when the helices were suspended in polar organic solvents such as alcohol (ethanol, methanol, HFIP) or acetonitrile. TEM images of ~1 nm THPC stabilized GNPs adsorbed on silica nanohelices are shown in Figure 2a. Such hybrid nanohelices were stable in water, and the size of these GNPs showed no change even after 1 week and eventually grew to 2–3 nm after a month. When these nanocomposite structures were put into polar organic solvents such as alcohol (ethanol, methanol, HFIP) or acetonitrile, the size of the metal particles increased to ~5 nm within days (Supporting Information). Figure 3a–d illustrates this growing process in

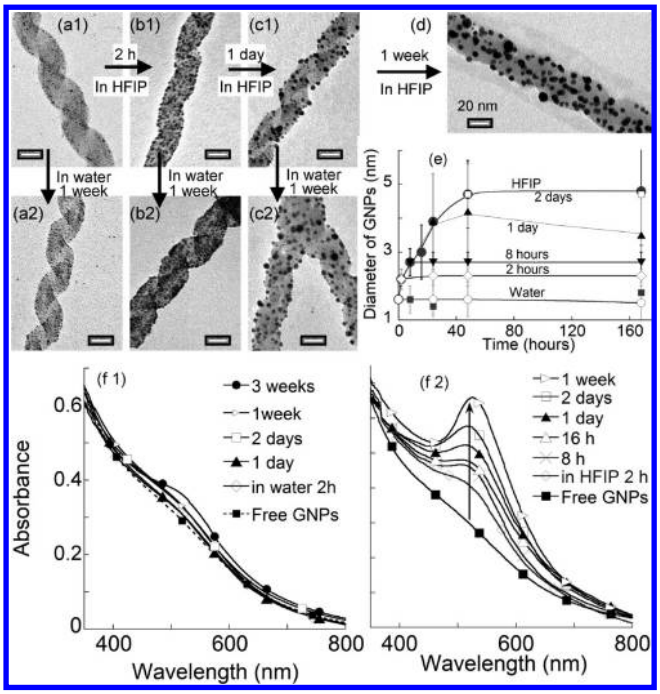

Figure 3. TEM images of GNPs at the surface of silica nanohelices and their growth process (a–d), the plot of their diameter vs time (e), and UV–visible spectra (f). GNPs with ~1 nm diameter were adsorbed on the surface of silica helices (a1). The diameter of GNPs increased to around 5 nm in a suspension of HFIP (b1, c1, d). Those kept in water for a week did not grow in size (a2). Those which were first suspended in HFIP and then transferred in water stopped their growth immediately after the transfer (b2, c2). Free GNPs kept in HFIP (□) and GNPs/silica nanohelices kept in water (×) (e) show no change of GNP sizes. UV spectra of the samples kept in water (f1) and kept in HFIP (f2).

HFIP: the GNPs immobilized on the surface of silica nanohelices grow quickly to ~2 nm after 2 h (Figure 3b1), ~3 nm after 1 day (Figure 3c1), and then to about 5 nm after 1 week (Figure 3d) in a suspension of HFIP. In the literature, some examples have shown that small GNPs could grow on a fiber or particle surface.[30,29,68] However, in these cases, the authors used polar organic solvent as a reducing agent of the free metallic cations which were still present in solution.[69,70] In the present case, at the condition in which the nanohelices are stored, no free gold ions are present because the excess of GNPs and Au salt were completely washed away by water before solvent replacement. Clearly the growth of GNPs is due to the coalescence of smaller GNPs via an Ostwald ripening process.[71,72]

Such a growth could be stopped as soon as the solvent was exchanged by water (Figures 3a2, 2b2, and 2c2), and their size remained identical even after a week (Figure 3e, dotted line). Figure 3e shows the variation of the particle diameter with time. The free GNPs alone as well as the GNPs/silica nanocomposite

dx.doi.org/10.1021/jp307784m | J. Phys. Chem. C 2012, 116, 23143–23152

suspension in water did not show the growth process (Figure 3e, black squares and open circles, respectively).

Small GNPs (<2 nm) do not show a localized surface plasmon resonance (LSPR) band (Figure 3f) owing to the onset of quantum size effects observed for NP < 3 nm.[73] The color of the suspension of such GNPs as well as those adsorbed at the surface of nanohelices is brown. When the GNPs/silica nanohelice samples were kept in water, no LSPR peak appeared even after 1 week; it took 3 weeks to see a weak band appear (Figure 3f1) which is in good agreement with the GNP size observed with TEM. However, in HFIP, a broad SPR band appeared at 526 nm after 2 h (Figure 3f2). As the GNPs grew larger (~5 nm), this LSPR band increased in intensity, became sharper, and the color of the suspension turned red.[74,75] The plasmon absorption band of the metal nanoparticle due to collective oscillation of the free electrons confined to the surface is sensitive to changes in the size of the particle, and as the diameter gets larger, the energy required to collectively excite the motion of the surface plasmon electrons decreases.

For free GNPs with diameters from 3.5 to 37 nm, this energy corresponds to a maximum absorbance at around 524 nm.[66,68] This process also depends on the shape of GNPs, the chemical nature of the stabilizer, as well as the surrounding medium.[76−78] Interestingly, in the present case, upon their adsorption on the helix surface and by consequence of their positioning in close proximity to one another, the LSPR of the GNPs did not show a notable shift and remained at around 525 nm.[79−82]

The Particle Growth on the Surface of Silica Helices by Addition of Gold Salt and Reducing Agent. The particle growth on the surface of silica helices was also promoted by the addition of a growth solution containing both a gold salt and a reducing agent. The suspension of 500 μL silica nanohelices coated with THPC-GNPs was sonicated first, and then, various volumes (10−200 μL) of the growth solution composed of a 1:1 volume equivalent of 1 mM $KAuCl_4$ solution and 4.8 mM L-ascorbic acid (LAA) solution were added. The color of the solution immediately turned reddish brown. TEM images of these silica nanohelices are shown in Figure 3a. With the increasing quantity of the growth solution, the size of the GNPs increased homogeneously and continuously up to around 5 nm keeping a spherical shape. When the added volume of growth solutions was larger than 100 μL, the size of the particles became extremely heterogeneous, leading to highly non-spherical particles.

UV−vis spectra of GNPs on the silica substrate for various Au^{3+} salt concentrations are shown in Figure 4c. As mentioned above, no LSPR peak is observed for the silica suspension without added growth solution (GNP diameter ~1 nm). Upon addition of 10−25 μL growth solutions, a broad LSPR peak appeared at 530 nm. This peak became more pronounced with addition of growth solution (50 and 100 μL).

This method therefore provides an easy control of the size of ultrasmall GNPs (USGNPS) on silica substrates. The growth process is a kinetically controlled phenomenon; indeed, the addition of the gold solution in three consecutive steps, e.g., 10, 20, and 20 μL, instead of a single shot of 50 μL in a single step into 100 μL of the silica suspension did not lead to the same results. The latter showed relatively homogeneous adsorption of larger size GNPs, whereas the former showed separation between helices heavily covered by large GNPs and those which were poorly covered (Figure S2 in the Supporting Information).

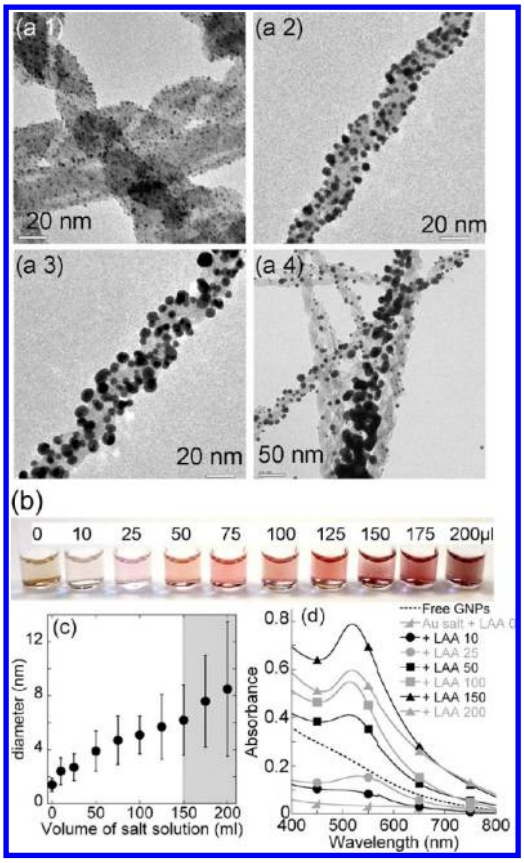

Figure 4. (a1−a4) TEM images of the growth process of GNPs at the surface of silica nanohelices; the volumes of growth solution used for GNP growth were 10 μL (a1), 50 μL (a2), 100 μL (a3), and 200 μL (a4); (b) picture illustrating the various color changes; (c) variation of the GNP diameter with the added volume of growth solution (diameter measurements were performed on an average of 500 particles; and (d) corresponding UV−visible spectra.

Larger GNPs Deposited on the Silica Nanohelices. The direct growth process of GNPs on the helices could not provide particles with a homogeneous size larger than 5 nm; we therefore undertook their separated synthesis followed by their deposition on the chemically modified surface. We subsequently investigated how the confinement of these large GNPs (10−14 nm) on the surface of silica nanohelices could affect the LSPR signals. For this study, we used citrate-stabilized GNPs in the presence of silica nanohelices APTES-functionalized with. Figure 5 shows silica nanohelices coated with GNPs of various sizes (10, 12, and 14 nm) and their corresponding absorption band (LSPR peak).

GNP/Silica Nanohelices Used as a SERS Substrate. As commonly demonstrated, the localized SPR exhibited by noble metal nanoparticles beyond a certain size can be exploited to induce the SERS effect. It has been shown that the gold surface morphology has an important effect on the enhancement of the Raman signal.[55] We therefore studied the potentiality of these hybrid helices as substrates for SERS measurements directly in an aqueous suspension. Figure 6 is illustrative of such an application and shows the SERS spectrum of benzenethiol (BT) used as a molecular probe adsorbed on these hybrid nanostructures in suspension (for various diameters of spherical GNPs). This spectrum is characteristic of BT adsorbed on Au substrate.[83−85] The main bands are observed at 1075, 1025, and

dx.doi.org/10.1021/jp307784m | J. Phys. Chem. C 2012, 116, 23143−23152

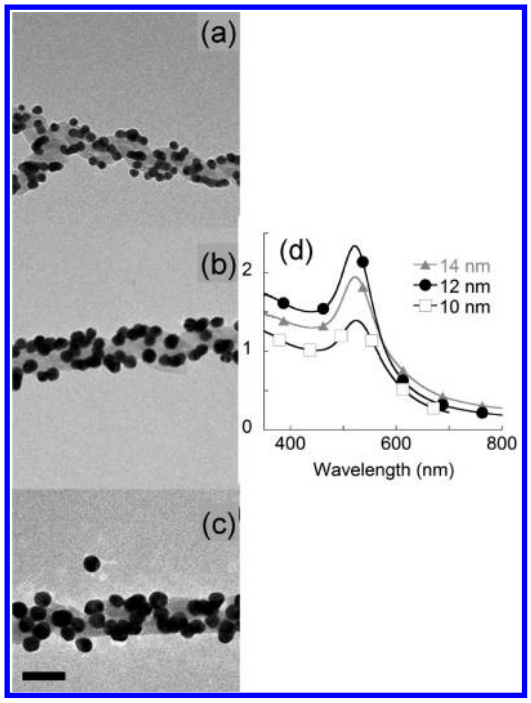

Figure 5. Silica nanohelices with GNPs: (a) 10 nm, (b) 12 nm, (c) 14 nm. Scale bar 50 nm. (d) UV–vis spectra of the hybrid suspension.

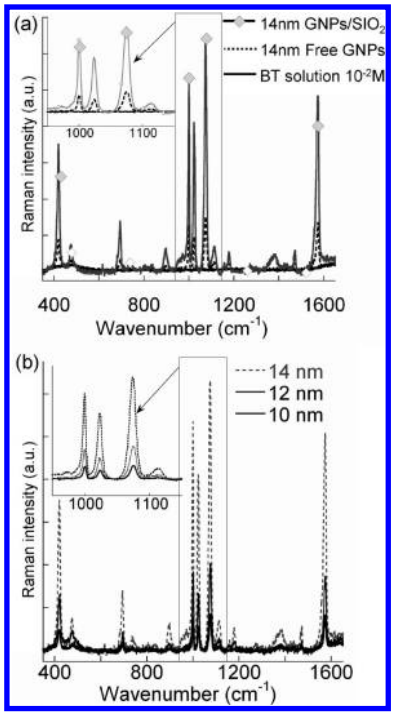

Figure 6. Raman and SERS spectra of benzenethiol. (a) Comparing the Raman spectrum of 10^{-2} M BT aqueous solution, the SERS spectrum of 10^{-6} M BT in 14 nm GNP colloid solution, and that of 10^{-6} M BT in the presence of GNP/silica nanohelix hybrid structures; (b) SERS spectra of 10^{-6} M BT adsorbed on GNP/silica nanohelix hybrid structures with different diameters (10, 12, and 14 nm). λ_{ex} = 633 nm.

1000 cm^{-1}, assigned to ν_1, ν_{18a}, and ν_{12} ring modes of BT, respectively.[84]

SERS spectra of 10^{-6} M BT solution mixed either with free GNP colloid solution or with GNP/silica nanohelix hybrid structures are shown in Figure 6a. In the absence of GNPs, no signal was detected even at concentrations as high as 10^{-2} M (see Figure 6a). Indeed, the lowest detection limit for the concentration of BT by Raman scattering is 10^{-1} M. Meanwhile, highly enhanced Raman signals were observed in the presence of GNPs.

Figure 6a also illustrates the crucial contribution of the helical silica in the suspension. Indeed, when these GNPs were adsorbed and organized on the surface of silica nanohelices, they generates hot spots, and a further enhancement of Raman signal was observed. The enhancement is more important for larger particles (14 nm), probably because the plasmon band for larger particles is more intense (Figure 4). The organization of GNPs can also be different. As it can be clearly seen in Figure 5, the GNPs on the silica helices are organized in 2D at the outer surface of silica helices, and the interparticle distances vary in the average between close contact to 10 nm, all of these close contacts generating hot spots favorable to the enhancement. These systems exhibit higher enhancement (about 5 times) than the free GNPs are in free solution. We then investigated the effect of the BT concentration on the Raman spectra for GNPs with different sizes. Figure 7a shows the variation of the intensity (deduced from the intensity of the band at 1000 cm^{-1}) with the BT concentration.

Globally, the enhancement of BT spectra decreases with increasing concentration. This tendency seems to be more pronounced for the biggest nanoparticles.

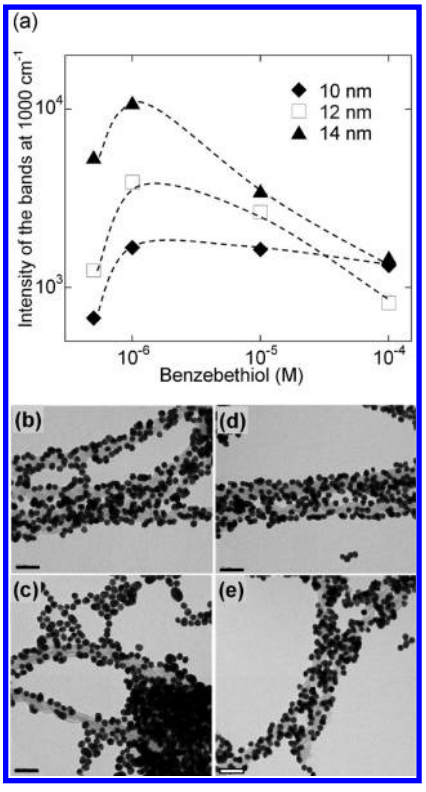

Figure 7. (a) Intensity of the bands at 1000 cm^{-1} with concentration of BT. All the SERS spectra were recorded with the same laser power (5 mW) and same accumulation time (120 s); TEM images of silica helices with 14 nm GNPs and (b) 10^{-6} M and (c) 10^{-5} M BT. TEM images of silica helices with 10 nm GNPs and (d) 10^{-6} M and (e) 10^{-5} M BT. Desorption and aggregation of GNPs (14 nm) is clearly seen for a high concentration of BT (c). Scale bar 50 nm.

dx.doi.org/10.1021/jp307784m | J. Phys. Chem. C 2012, 116, 23143–23152

Such a variation of the SERS intensity as a function of BT concentration can be explained considering the TEM images of the systems (Figure 7b–e) as well as the macroscopic aspects of the suspensions. The smallest GNPs (10 nm) show a homogeneous adsorption on the surface of silica nanohelices at all studied concentrations (10^{-7}–10^{-4} M), whereas the larger ones (12 and 14 nm) show desorption from the silica and seem to aggregate at concentrations beyond 10^{-5} M (Figure 7c). For these BT concentrations, the color of the solutions changes from pink to dark blue, and the LSPR peak becomes broader and red-shifted (Figure S3 in the Supporting Information).

The higher ionic strength (higher concentrations of sodium citrate) required for the preparation of smaller particles for stabilization gives more anionic surface charge to the smaller particles than to the larger ones which may explain their better adsorption.

The decrease in SERS intensity with increasing BT concentration (Figure 7c) could be explained by the combined effect of (1) saturation of the adsorption sites at higher BT concentration and (2) the shift of LSPR peak induced by the aggregation of the GNPs at high BT concentration, which leads to the decrease of the Raman signals. These systems are definitely dedicated to the chemical sensing of low concentrations of active molecules.

CONCLUSION

Silica nanohelices synthesized from the organic self-assemblies of 16–2–16 L-tartrate amphiphiles by sol–gel transcription were functionalized with APTES or MPTES and GNP/silica nanohelix hybrid structures were obtained with GNPs of various sizes. The quantity of adsorbed GNPs and their homogeneity depend on various factors such as the GNP size, silica surface functional group (APTES or MPTES), as well as the chemical nature of the stabilizing agents. When the nanohybrid structures based on small (1–2 nm) GNPs stabilized by THPC were kept in organic solvents such as alcohol, GNPs adsorbed at the surface of silica nanohelices grew to 5–6 nm within days characteristic of Ostwald ripening. On the other hand, in water suspension, such a growth was only observed upon addition of a growth solution containing both a gold salt and a reducing agent. In this case, the diameter of GNPs homogeneously increased with the concentration of gold salt up to around 5 nm. Beyond this concentration, the size of the particles became extremely heterogeneous, leading to highly non-spherical particles.

The surface plasmon resonance intensity of the nanohybrid systems increased with particle size. For the GNPs with 10–14 nm diameter, these hybrid systems clearly showed a surface enhanced effect on Raman spectroscopy. The 3D network of these GNP/silica nanohelix hybrid structures can therefore be used as ultrasensitive chemical and biological sensors for the liquid phase. Up to now, typical SERS substrates reported in the literature were made from noble metal nanoparticles assembled on planar surfaces or a patterned surface. Using these functionalized 3D silica nanohelices, we design a novel type of SERS substrate based on the 3D gel network of GNP/silica nanohelix hybrid nanostructures. Compared to the commonly used 2D SERS substrates, the use of such 3D network systems can open a totally new perspective toward high detection of molecules of interest through accumulation under flow.

EXPERIMENTAL PROCEDURES

Synthesis of 16–2–16 Tartrate and Gel Formation. The 16–2–16 amphiphiles with tartrate counterions were synthesized according to previously published data.[37,86]

Preparation of Silica Nanohelices. Once adequate aging time of the gels is reached, these organic self-assemblies are used as templates to prepare silica nanostructures through a sol–gel transcription procedure. In a typical preparation, 500 μL of 5 wt % tetraethylorthosilicate (TEOS) is prehydrolyzed in water (pH 6) for 12 h at room temperature before each run, and then added to 500 μL of 1 or 5 mM organic gels with various aging times (typically 20 days for nanohelices and more than 45 days for closed tubules). The reaction mixture was vortexed (2000 rpm) for a few seconds, and then kept at 20 °C for more than 36 h. The samples were then thoroughly washed with ethanol to remove all organic components and excess TEOS. Typically, from 0.36 mg of organic gels, we obtained 1.2 ± 0.2 mg of silica nanohelices. This procedure led us to the average 0.12 wt % of silica helices from 1 mM organic gel and 3.5 wt % silica helices from 5 mM initial organic gel.

Functionalization of Silica Nanohelices. The silica nanohelices were then functionalized via a surface chemical modification with (3-aminopropyl)triethoxysilane (APTES) or (3-mercaptopropyl)triethoxysilane (MPTES). The washed silica nanohelices were redispersed in water (pH 6), and 25 μmol of APTES (or MPTES) per 1.2 mg of silica nanohelices were added. The reaction mixture was submitted to ultrasonication for 2 h and then kept in water overnight at 85 °C.

Synthesis of GNPs. In order to get various sizes of GNPs between 1.2 and 14 nm, three types of stabilizers were used: citrate, cetyltrimethylammonium bromide (CTAB), and tetrakis (hydroxymethyl)phosphonium chloride (THPC).

Citrate-Stabilized GNPs. Au particles of about 10 nm were synthesized according to the method reported by Frens et al.[87–89] All the glassware used in these experiments was cleaned with aqua regia (a 1:3 mixture of concentrated nitric acid and hydrochloric acid) and then immediately rinsed with ultrapure water. In a typical preparation, 40 mL of ultrapure water was boiled in advance and 10 mL of 0.1 wt % potassium tetrachloroaurate ($KAuCl_4$) aqueous solution was added to the boiling water. As the gold solution reached 100 °C, 5 mL of 0.9 wt % of trisodium citrate solution was added under vigorous stirring. After the addition of citrate in the gold salt solution, the color turned blue, dark purple, and finally dark red in 20 min, indicating the formation of GNPs. The GNP size could be controlled by varying the $[Au^{3+}]/[citrate]$ ratio (0.17 for 10 nm, 0.28 for 12 nm, and 0.37 for 14 nm).

THPC-Stabilized GNPs. The smallest Au nanoparticles with a diameter of around 1–2 nm were prepared by reduction of $KAuCl_4$ with tetrakis(hydroxymethyl)phosphonium chloride (THPC) using a modification of the work reported by Duff et al.[90,91] An aqueous solution of sodium hydroxide (36 mL, 6.6 mM) and 0.8 mL of a THPC solution (67.0 mM) were mixed in a flask and vigorously stirred for 25 min. The aqueous solution of $KAuCl_4$ (1.35 mL, 1 wt %) was quickly added to the THPC/NaOH mixture and left under stirring for 30 min. The color of the solution rapidly changed from colorless to brown. The GNP suspension was then stored in the refrigerator for at least 3 days before use.[92]

CTAB-Stabilized GNPs. The positively charged nanoparticles were synthesized by using a seed-mediated growth method in the presence of cetyltrimethylammonium bromide (CTAB) as

a cationic capping agent.[93−95] The preparation process has several steps: at first, the small seeds with a 3.5 nm diameter are synthesized by chemical reduction of gold salt with a strong reducing agent (sodium borohydride) in the presence of a capping agent (citrate); then, these seeds are added to a growth solution containing more metal salt, a weak reducing agent (e.g., ascorbic acid), and CTAB. For the gold seeds synthesis, 0.25 mM $HAuCl_4$ and 0.25 mM trisodium citrate were dissolved in 20 mL of ultrapure water. Ice cold $NaBH_4$ aqueous solution (0.6 mL, 0.1 M) was added to the mixture under stirring. The solution immediately turned red-orange, indicating the formation of GNPs with a diameter of 3.5 ± 0.7 nm.[96] The seeds were stored at 25 °C for 3 h before use to allow excess borohydride to be decomposed by water.

For the growth of GNPs, a growth solution (18 mL) containing 0.25 mM $HAuCl_4$ and 0.08 M CTAB was prepared by gentle heating and to it added 100 μL of 0.1 M L-ascorbic acid solution, Finally, 2 mL of the 3.5 nm seed solution was added to the above mixture and kept under vigorous stirring for 10 min. The final color was dark red, and the particle size was 9 ± 1.5 nm. These GNPs could be used soon after the synthesis and were stable for a month due to the presence of a bilayer of the CTAB stabilizer.

Citrate-Stabilized or THPC-Stabilized GNPs on Silica Helices. Typically, the optimal conditions are as follows: to use silica helices transcribed from 1 mM organic gels, these helices should also exhibit a high APTES coverage density. The functionalized silica helices are then dispersed in water; about 0.12 wt % of the silica nanohelix (10−50 μL) suspension in water is added into the GNP suspension (the Au concentration in terms of gold salt is 0.5 mM for citrate stabilized GNPs and 0.97 mM for THPC stabilized GNPs, 200 μL) under ultrasonication. Upon addition of the silica nanohelices into the 10 nm citrate−GNP water solution, the color of the solution turned from dark red to pink. In the case of THPC-GNPs, a higher quantity of silica helices was used, as the smaller GNPs can coat more efficiently the silica helix surface, up to ∼200 μL of 0.12 wt % silica for 200 μL of GNP solution.

CTAB-Stabilized GNPs on MPTES Functionalized Silica Helices (in Ethanol). We removed CTAB adsorbed on the GNP surface via a procedure from ref 57. This is done by adding ethanol to the solution; typically 10−50 μL of a MPTES-functionalized silica nanohelix suspension in water (0.12 wt %) is dispersed into 500 μL of a CTAB−GNP suspension (0.25 mM of Au element) under ultrasonication. 500 μL of ethanol is then added to the suspension in order to break the CTAB bilayer adsorbed on the GNPs and let them bind to the surface of silica through the thiol group. The sonication is continued for 10 min, and the overall suspension color turned pink. The GNP/silica nanohelix samples are collected by centrifugation. This process is repeated to allow a higher concentration of GNPs immobilized onto the silica surface.

Characterization. The study of localized surface plasmon resonance was performed with a Cary 300 UV−vis spectrometer. The data were recorded with a 1.0 nm data interval and a 600 nm/min scan rate. Quartz cuvettes with an optical path length of 10 mm were used for measurements. TEM was performed at room temperature on a Philips EM 120 electron microscope operating at 120 kV, and the images were collected by a 2k × 2k Gatan ssCCD camera. Drops of diluted dispersions of the hybrids were deposited on carbon-film-coated 400-mesh copper grids. The excess liquid was blotted with filter paper. Benzenethiol (BT, from Sigma-Aldrich) was used as a probe to quantify the enhancement of Raman scattering by the new 3D helical structures coated with gold nanoparticles. BT diluted solutions were prepared in water from a 10^{-3} M stock solution. The ratio of SERS substrate and BT was 9/1 (v/v). Raman and SERS spectra were recorded with a Labram HR800 (Horiba JobinYvon) using a 633 nm excitation of a helium/neon ion laser. The laser beam was focused on the sample using a 10× objective. The laser power was fixed at 5 mW. The accumulation times were 5 and 120 s for pure BT and diluted BT, respectively.

Electron tomography (ET) experiments have been carried out on representative silica helices by using a JEOL 2100F TEM/STEM electron microscope operating at 200 kV, equipped with a TRIDIEM postcolumn imaging filter and a Cs probe corrector. Before observations, the samples were deposited on a holey carbon membrane copper grid which was previously cleaned using a H_2/Ar plasma gas using a Solarus PlasmaCleaner. The acquisition of the tilt series was performed in the classical TEM mode with the Digital Micrograph software which provides an automated acquisition of the tilt series by varying the tilt angle step by step and by controlling the defocusing and the specimen drift at each tilt angle. Using a high tilt sample holder from the GATAN Company, TEM tilt series were acquired between 75 and −75°, with a 1.5° equal tilt increment. As a result, the total number of projections was about 100, for a recording duration of about 45 min. Once the acquisition of the tilt series completed, the images were roughly aligned using a cross correlation algorithm, followed by a fine alignment performed in the IMOD software[97] where the gold nanoparticles located on the silica helices were used as fiducial markers. The 3D reconstructions were computed by using algebraic reconstruction techniques (ART)[98] implemented in the TomoJ software[99] with 20 iterations. Visualization and quantitative analysis of the final volumes were carried out by using Slicer (http://www.Slicer3D.org) and ImageJ softwares.

■ ASSOCIATED CONTENT

Supporting Information

Figure S1 shows the effect of the method of addition of gold salt and reducing agent in several steps (a−c) and in a single step (d) on the GNP coating on the silica nanohelices. Figure S2 shows the TEM images comparing (a) CIT-stabilized GNPs added to silica nanohelices and (b) silica nanohelices added to GNPs. Figure S3 shows the UV−vis spectra comparing GNPs/SiO_2 (dotted line) and adsorption of 10^{-4} M BT on GNPs/SiO_2 (straight line). This material is available free of charge via the Internet at http://pubs.acs.org.

■ AUTHOR INFORMATION

Corresponding Author

*E-mail: r.oda@iecb.u-bordeaux.fr.

Notes

The authors declare no competing financial interest.

■ ACKNOWLEDGMENTS

R.O. and M.-H.D. thank Dr. B. Desbat (CBMN) and Dr. I. Florea (IPCMS) for helpful discussion. S.L. acknowledges the GSV group of the ISM laboratory (UMR 5255, CNRS/Université de Bordeaux) for access to the Raman spectrometer. The authors want to gratefully acknowledge the financial support of the "Agence Nationale de la Recherche" grant no.

ANR-10-BLAN-0813 (NANOSPRINGS). S.M. and O.E. gratefully acknowledge the financial support for the French Network for Transmission Electron Microscopy (METSA).

REFERENCES

(1) Sada, K.; Takeuchi, M.; Fujita, N.; Numata, M.; Shinkai, S. *Chem. Soc. Rev.* **2007**, *36* (2), 415−435.
(2) Llusar, M.; Sanchez, C. *Chem. Mater.* **2008**, *20* (3), 782−820.
(3) Sanchez, C.; Arribart, H.; Guille, M. M. G. *Nat. Mater.* **2005**, *4* (4), 277−288.
(4) Pappas, J. L. *J. Nanosci. Nanotechnol.* **2005**, *5* (1), 120−130.
(5) Che, S. *J. Nanosci. Nanotechnol.* **2006**, *6* (6), 1557−1564.
(6) Wu, X. W.; Ruan, J. F.; Ohsuna, T.; Terasaki, O.; Che, S. N. *Chem. Mater.* **2007**, *19* (7), 1577−1583.
(7) Moreau, J. J. E.; Vellutini, L.; Man, M. W. C.; Bied, C. *J. Am. Chem. Soc.* **2001**, *123* (7), 1509−1510.
(8) Moreau, J. J. E.; Vellutini, L.; Man, M. W. C.; Bied, C. *Chem.—Eur. J.* **2003**, *9* (7), 1594−1599.
(9) Jung, J. H.; Shinkai, S.; Shimizu, T. *Nano Lett.* **2002**, *2* (1), 17−20.
(10) Okamoto, K.; Shook, C. J.; Bivona, L.; Lee, S. B.; English, D. S. *Nano Lett.* **2004**, *4* (2), 233−239.
(11) Nakamura, H.; Matsui, Y. *J. Am. Chem. Soc.* **1995**, *117* (9), 2651−2652.
(12) Sone, E. D.; Zubarev, E. R.; Stupp, S. I. *Angew. Chem., Int. Ed.* **2002**, *41*, 1705−1709.
(13) Goren, M.; Qi, Z. G.; Lennox, R. B. *Chem. Mater.* **2000**, *12* (5), 1222−1228.
(14) Shenton, W.; Pum, D.; Sleytr, U. B.; Mann, S. *Nature* **1997**, *389* (6651), 585−587.
(15) Davis, S. A.; Burkett, S. L.; Mendelson, N. H.; Mann, S. *Nature* **1997**, *385* (6615), 420−423.
(16) Kim, S. S.; Zhang, W. Z.; Pinnavaia, T. J. *Science* **1998**, *282* (5392), 1302−1305.
(17) Shimizu, T.; Masuda, M.; Minamikawa, H. *Chem. Rev.* **2005**, *105* (4), 1401−1443.
(18) Lopez, P. J.; Gautier, C.; Livage, J.; Coradin, T. *Curr. Nanosci.* **2005**, *1* (1), 73−83.
(19) Pouget, E.; Dujardin, E.; Cavalier, A.; Moreac, A.; Valery, C.; Marchi-Artzner, V.; Weiss, T.; Renault, A.; Paternostre, M.; Artzner, F. *Nat. Mater.* **2007**, *6* (6), 434−439.
(20) Menzel, H.; Horstmann, S.; Behrens, P.; Barnreuther, B.; Krueger, I.; Jahns, M. *Chem. Commun.* **2003**, *24*, 2994−2995.
(21) Annenkov, V. V.; Patwardhan, S. V.; Belton, D.; Danilovtseva, E. N.; Perry, C. C. *Chem. Commun.* **2006**, *14*, 1521−1523.
(22) Ono, Y.; Nakashima, K.; Sano, M.; Kanekiyo, Y.; Inoue, K.; Hojo, J.; Shinkai, S. *Chem. Commun.* **1998**, *14*, 1477−1478.
(23) Jung, J. H.; Ono, Y.; Shinkai, S. *Chem.—Eur. J.* **2000**, *6* (24), 4552−4557.
(24) Jung, J. H.; Kobayashi, H.; Masuda, M.; Shimizu, T.; Shinkai, S. *J. Am. Chem. Soc.* **2001**, *123* (36), 8785−8789.
(25) Minakuchi, H.; Nakanishi, K.; Soga, N.; Ishizuka, N.; Tanaka, N. *Anal. Chem.* **1996**, *68* (19), 3498−3501.
(26) Sonnenburg, K.; Adelhelm, P.; Antonietti, M.; Smarsly, B.; Noske, R.; Strauch, P. *Phys. Chem. Chem. Phys.* **2006**, *8* (30), 3561−3566.
(27) Ihara, H.; Takafuji, M.; Sakurai, T. *Self-Assembled Nanobiomaterials*; American Scientific Publishers: 2004; Vol. *9*.
(28) Brizard, A.; Oda, R.; Huc, I. In *Low Molecular Mass Gelators: Design, Self-Assembly, Function*; Springer-Verlag: Berlin, 2005; Vol. *256*, pp 167−218.
(29) Patzke, G. R.; Krumeich, F.; Nesper, R. *Angew. Chem., Int. Ed.* **2002**, *41* (14), 2446−2461.
(30) Singh, J. P.; Liu, D. L.; Ye, D. X.; Picu, R. C.; Lu, T. M.; Wang, G. C. *Appl. Phys. Lett.* **2004**, *84* (18), 3657−3659.
(31) Korgel, B. A. *Science* **2005**, *309* (5741), 1683−1684.
(32) Gao, P. X.; Mai, W. J.; Wang, Z. L. *Nano Lett.* **2006**, *6* (11), 2536−2543.
(33) Yang, Y. G.; Suzuki, M.; Fukui, H.; Shirai, H.; Hanabusa, K. *Chem. Mater.* **2006**, *18* (5), 1324−1329.
(34) Li, H. T.; Li, B. Z.; Chen, Y. L.; Wu, X. J.; Zhang, J.; Li, Y.; Hanabusa, K.; Yang, Y. G. *Mater. Chem. Phys.* **2009**, *118* (1), 135−141.
(35) Delclos, T.; Aime, C.; Pouget, E.; Brizard, A.; Huc, I.; Delville, M. H.; Oda, R. *Nano Lett.* **2008**, *8* (7), 1929−1935.
(36) Oda, R.; Artzner, F.; Laguerre, M.; Huc, I. *J. Am. Chem. Soc.* **2008**, *130* (44), 14705−14712.
(37) Oda, R.; Huc, I.; Schmutz, M.; Candau, S. J.; MacKintosh, F. C. *Nature* **1999**, *399* (6736), 566−569.
(38) Brizard, A.; Aime, C.; Labrot, T.; Huc, I.; Berthier, D.; Artzner, F.; Desbat, B.; Oda, R. *J. Am. Chem. Soc.* **2007**, *129* (12), 3754−3762.
(39) Hutter, E.; Fendler, J. H. *Adv. Mater.* **2004**, *16* (19), 1685−1706.
(40) Toderas, F.; Baia, M.; Baia, L.; Astilean, S. *Nanotechnology* **2007**, *18* (25).
(41) McMahon, J. M.; Henry, A. I.; Wustholz, K. L.; Natan, M. J.; Freeman, R. G.; Van Duyne, R. P.; Schatz, G. C. *Anal. Bioanal. Chem.* **2009**, *394* (7), 1819−1825.
(42) Aslan, K.; Lakowicz, J. R.; Geddes, C. D. *J. Phys. Chem. B* **2005**, *109* (13), 6247−6251.
(43) Aslan, K.; Leonenko, Z.; Lakowicz, J. R.; Geddes, C. D. *J. Phys. Chem. B* **2005**, *109* (8), 3157−3162.
(44) Freeman, R. G.; Grabar, K. C.; Allison, K. J.; Bright, R. M.; Davis, J. A.; Guthrie, A. P.; Hommer, M. B.; Jackson, M. A.; Smith, P. C.; Walter, D. G.; et al. *Science* **1995**, *267* (5204), 1629−1632.
(45) Nikoobakht, B.; El-Sayed, M. A. *J. Phys. Chem. A* **2003**, *107* (18), 3372−3378.
(46) Tao, A.; Kim, F.; Hess, C.; Goldberger, J.; He, R. R.; Sun, Y. G.; Xia, Y. N.; Yang, P. D. *Nano Lett.* **2003**, *3* (9), 1229−1233.
(47) Orendorff, C. J.; Gole, A.; Sau, T. K.; Murphy, C. J. *Anal. Chem.* **2005**, *77* (10), 3261−3266.
(48) Hayakawa, T.; Usui, Y.; Bharathi, S.; Nogami, M. *Adv. Mater.* **2004**, *16* (16), 1408−1412.
(49) Hirsch, L. R.; West, J. L.; Jackson, J. B.; Lee, A.; Halas, N. J. *Ieee In 25th Annual International Conference of the IEEE-Engineering-in-Medicine-and-Biology-Society*, Cancun, Mexico, 2003; Vol. *25*, pp 3442−3443.
(50) Sershen, S. R.; Westcott, S. L.; Halas, N. J.; West, J. L. *J. Biomed. Mater. Res.* **2000**, *51* (3), 293−298.
(51) Loo, C.; Lowery, A.; Halas, N. J.; West, J.; Drezek, R. *Nano Lett.* **2005**, *5* (4), 709−711.
(52) Duan, G. T.; Cai, W. P.; Luo, Y. Y.; Li, Y.; Lei, Y. *Appl. Phys. Lett.* **2006**, *89* (18).
(53) Pazos-Perez, N.; Ni, W. H.; Schweikart, A.; Alvarez-Puebla, R. A.; Fery, A.; Liz-Marzan, L. M. *Chem. Sci.* **2010**, *1* (2), 174−178.
(54) Shen, Y. F.; Wang, J. B.; Kuhlmann, U.; Hildebrandt, P.; Ariga, K.; Mohwald, H.; Kurth, D. G.; Nakanishi, T. *Chem.—Eur. J.* **2009**, *15* (12), 2763−2767.
(55) Im, H.; Bantz, K. C.; Lindquist, N. C.; Haynes, C. L.; Oh, S. H. *Nano Lett.* **2010**, *10* (6), 2231−2236.
(56) Hu, M. S.; Chen, H. L.; Shen, C. H.; Hong, L. S.; Huang, B. R.; Chen, K. H.; Chen, L. C. *Nat. Mater.* **2006**, *5* (2), 102−106.
(57) Zhang, S. Z.; Ni, W. H.; Kou, X. S.; Yeung, M. H.; Sun, L. D.; Wang, J. F.; Yan, C. H. *Adv. Funct. Mater.* **2007**, *17* (16), 3258−3266.
(58) Sai, V. V. R.; Gangadean, D.; Niraula, I.; Jabal, J. M. F.; Corti, G.; McIlroy, D. N.; Aston, D. E.; Branen, J. R.; Hrdlicka, P. J. *J. Phys. Chem. C* **2011**, *115* (2), 453−459.
(59) Tan, S. J.; Campolongo, M. J.; Luo, D.; Cheng, W. *Nat. Nanotechnol.* **2011**, *6* (5), 268−276.
(60) Ding, B.; Deng, Z.; Yan, H.; Cabrini, S.; Zuckermann, R. N.; Bokor, J. *J. Am. Chem. Soc.* **2010**, *132* (10), 3248−3249.
(61) Kuzyk, A.; Schreiber, R.; Fan, Z.; Pardatscher, G.; Roller, E. M.; Högele, A.; Simmel, F. C.; Govorov, A. O.; Liedl, T. *Nature* **2012**, *483*, 311−314.
(62) Chen, W.; Bian, A.; Agarwal, A.; Liu, L.; Shen, H.; Wang, L.; Xu, C.; Kotov, N. A. *Nano Lett.* **2009**, *9* (5), 2153−2159.
(63) Fan, Z.; Govorov, A. O. *J. Phys. Chem. C* **2011**, *115* (27), 13254−13261.

(64) Slocik, J. M.; Govorov, A. O.; Naik, R. R. *Nano Lett.* **2011**, *11* (2), 701−705.
(65) Westcott, S. L.; Oldenburg, S. J.; Lee, T. R.; Halas, N. J. *Langmuir* **1998**, *14* (19), 5396−5401.
(66) Vogel, W.; Duff, D. G.; Baiker, A. *Langmuir* **1995**, *11* (2), 401−404.
(67) Yong, K. T.; Sahoo, Y.; Swihart, M. T.; Prasad, P. N. *Colloids Surf., A* **2006**, *290* (1−3), 89−105.
(68) Yong, K. T.; Swihart, M. T.; Ding, H.; Prasad, P. N. *Plasmonics* **2009**, *4* (2), 79−93.
(69) Kim, J. H.; Bryan, W. W.; Chung, H. W.; Park, C. Y.; Jacobson, A. J.; Lee, T. R. *ACS Appl. Mater. Interfaces* **2009**, *1* (5), 1063−1069.
(70) Radloff, C.; Vaia, R. A.; Brunton, J.; Bouwer, G. T.; Ward, V. K. *Nano Lett.* **2005**, *5* (6), 1187−1191.
(71) Ratke, L.; Voorhees, P. W. *Growth and coarsening*; Springer: Berlin, New York, 2002; p 295.
(72) Stabel, A.; Heinz, R.; Deschryver, F. C.; Rabe, J. P. *J. Phys. Chem.* **1995**, *99* (2), 505−507.
(73) Daniel, M. C.; Astruc, D. *Chem. Rev.* **2004**, *104* (1), 293−346.
(74) McLean, J. A.; Stumpo, K. A.; Russell, D. H. *J. Am. Chem. Soc.* **2005**, *127* (15), 5304−5305.
(75) Martin, M. N.; Basham, J. I.; Chando, P.; Eah, S. K. *Langmuir* **2010**, *26* (10), 7410−7417.
(76) Barbic, M.; Mock, J. J.; Smith, D. R.; Schultz, S. *J. Appl. Phys.* **2002**, *91* (11), 9341−9345.
(77) Kottmann, J. P.; Martin, O. J. F.; Smith, D. R.; Schultz, S. *Chem. Phys. Lett.* **2001**, *341* (1−2), 1−6.
(78) Mock, J. J.; Smith, D. R.; Schultz, S. *Nano Lett.* **2003**, *3* (4), 485−491.
(79) Hussain, I.; Graham, S.; Wang, Z. X.; Tan, B.; Sherrington, D. C.; Rannard, S. P.; Cooper, A. I.; Brust, M. *J. Am. Chem. Soc.* **2005**, *127* (47), 16398−16399.
(80) Link, S.; Mohamed, M. B.; El-Sayed, M. A. *J. Phys. Chem. B* **1999**, *103* (16), 3073−3077.
(81) Su, K. H.; Wei, Q. H.; Zhang, X.; Mock, J. J.; Smith, D. R.; Schultz, S. *Nano Lett.* **2003**, *3* (8), 1087−1090.
(82) El-Brolossy, T. A.; Abdallah, T.; Mohamed, M. B.; Abdallah, S.; Easawi, K.; Negm, S.; Talaat, H. *Eur. Phys. J.: Spec. Top.* **2008**, *153*, 361−364.
(83) Carron, K. T.; Hurley, L. G. *J. Phys. Chem.* **1991**, *95* (24), 9979−9984.
(84) Szafranski, C. A.; Tanner, W.; Laibinis, P. E.; Garrell, R. L. *Langmuir* **1998**, *14* (13), 3570−3579.
(85) Ren, B.; Picardi, G.; Pettinger, B.; Schuster, R.; Ertl, G. *Angew. Chem., Int. Ed.* **2005**, *44* (1), 139−142.
(86) Oda, R.; Huc, I.; Candau, S. J. *Chem. Commun.* **1997**, *21*, 2105−2106.
(87) Frens, G. *Nature (London), Phys. Sci.* **1973**, *241* (105), 20−22.
(88) Basu, S.; Ghosh, S. K.; Kundu, S.; Panigrahi, S.; Praharaj, S.; Pande, S.; Jana, S.; Pal, T. *J. Colloid Interface Sci.* **2007**, *313* (2), 724−734.
(89) Pramanik, S.; Banerjee, P.; Sarkar, A.; Bhattacharya, S. C. *J. Lumin.* **2008**, *128* (12), 1969−1974.
(90) Duff, D. G.; Baiker, A.; Edwards, P. P. *Langmuir* **1993**, *9* (9), 2301−2309.
(91) Duff, D. G.; Baiker, A.; Gameson, I.; Edwards, P. P. *Langmuir* **1993**, *9* (9), 2310−2317.
(92) Kim, J. H.; Bryan, W. W.; Lee, T. R. *Langmuir* **2008**, *24* (19), 11147−11152.
(93) Jana, N. R.; Gearheart, L.; Murphy, C. J. *Langmuir* **2001**, *17* (22), 6782−6786.
(94) Nikoobakht, B.; El-Sayed, M. A. *Chem. Mater.* **2003**, *15* (10), 1957−1962.
(95) Gole, A.; Murphy, C. J. *Chem. Mater.* **2004**, *16* (19), 3633−3640.
(96) Jana, N. R.; Gearheart, L.; Murphy, C. J. *J. Phys. Chem. B* **2001**, *105* (19), 4065−4067.
(97) Mastronarde, D. N. *J. Struct. Biol.* **1997**, *120* (3), 343−352.
(98) Gordon, R.; Bender, R.; Herman, G. T. *J. Theor. Biol.* **1970**, *29*, 477−481.
(99) Messaoudil, C.; Boudier, T.; Sorzano, C. O. S.; Marco, S. *BMC Bioinform.* **2007**, *8*, 288.